Theoretical Interpretation of the Photoelectron Spectra of $Al_3O_2^-$ and $Al_3O_3^-$

Tapan K. Ghanty[†] and Ernest R. Davidson*

Department of Chemistry, Indiana University, 800 E. Kirkwood Ave., Bloomington, Indiana 47405-7102

Received: July 26, 1999; In Final Form: September 23, 1999

Hartree−Fock (HF) and density functional theory (DFT) calculations have been used to determine the equilibrium geometries of the ground electronic state of Al_3O_2, Al_3O_3, and their corresponding negative ions. The calculated global minimum for Al_3O_2 has a "vee" shape of C_{2v} symmetry with a $(a_1)^1\ ^2A_1$ configuration. A kite-shaped structure of C_{2v} symmetry has been obtained as a local minimum with a $(b_2)^1\ ^2B_2$ configuration. The corresponding negative ions have also been found to be global and local minima, respectively, with $(a_1)^2\ ^1A_1$ and $(b_2)^2\ ^1A_1$ electron configurations. A higher energy trigonal bipyramidal D_{3h} structure has been found with a $^1A_1'\ (e')^4$ electron configuration. For $Al_3O_3^-$, the calculated global minimum has a bicyclic rectangular shape of C_{2v} symmetry with a $(b_2)^2\ ^1A_1$ configuration, whereas the corresponding neutral Al_3O_3 with a $(b_2)^1\ ^2B_2$ configuration has been found to be a local minimum. On the other hand, a kite shape of C_{2v} symmetry with a $(a_1)^1\ ^2A_1$ configuration has been found to be the global minimum of neutral Al_3O_3. The lowest triplet state of $Al_3O_3^-$ had a hexagonal shape of D_{3h} symmetry with a $(e')^2$ configuration. This triplet minimum has slightly higher energy than either of the singlet minima. Configuration interaction (CI) calculations have been performed using the DFT optimized geometries for the two lowest energy structures of $Al_3O_2^-$ and the two lowest energy structures of $Al_3O_3^-$ to determine the low lying vertical excited states of Al_3O_2 and Al_3O_3. Those results have been utilized to interpret the recently reported experimental photoelectron spectra of $Al_3O_2^-$ and $Al_3O_3^-$. On the basis of the present CI results, the symmetry of the states involved in the photoelectron peaks have been assigned for both spectra.

Introduction

In electronic structure calculations, electron correlation has a very important effect on structure and properties of atoms, molecules, or solids. The electron correlation[1] energy, defined as $E_{corr} = E_{exact} - E_{HF}$, usually changes in a chemical process by the same order of magnitude as the energy differences of chemical interest. Specifically, in photoelectron spectroscopy and electron momentum spectroscopy of molecules where electrons are removed from the inner valence shells, electron correlation plays an important role in explaining experimentally observed binding energy spectra.

Photoelectron spectroscopy is one of the direct probes of the core and valence electronic structure of molecules. The interpretation of photoelectron spectra has benefitted tremendously from simple molecular orbital (MO) models, like Hartree−Fock theory, which have been successful in accounting for the main features of photoelectron spectra in the outer valence region. Generally, there is one-to-one correspondence between the energies of the valence molecular orbitals and the main ionization peaks. However, simple MO theory cannot account for the lower intensity "extra" peaks that are very often observed.[2] These extra peaks are called correlation peaks (although they are also referred to as satellite peaks, shake-up peaks, or many body peaks) and have zero intensity in the Hartree−Fock model. It is precisely from the effect of electron correlation in atomic or molecular systems that these peaks gain intensity and appear in the photoelectron spectra. Recent benchmark configuration interactions (CI) calculations[3−8] have been able to interpret and predict the electron binding energy spectra of a number of molecular systems. Besides CI, other theoretical methods have also been used[9−11] to explain the main features in the photoelectron spectra of molecules.

In recent years, metal clusters have been the subject of several experimental and theoretical investigations[12,13] of the electronic structure and bonding, not only for the ground electronic state but also for their low lying excited electronic states. Because of the likely presence of a large number of closely spaced excited states, this is a rather challenging job. "Hypermetallic molecules" involving metal oxidation numbers less than normal valence expectations are now well documented experimentally[14−16] and have been extensively studied theoretically.[17−21] These species can be regarded as metal clusters bound ionically to a centrally located nonmetallic atom. Within this class of molecules Al_3O has been studied[8,14,17,19] both experimentally and theoretically. Very recently,[8] we calculated the geometries and electronic structures of Al_3O and its anion, and those results have been utilized to interpret the photoelectron spectrum of Al_3O^-.

Recently, the photoelectron spectra of $Al_3O_y^-$ ($y = 2, 3$) have been reported[22] at different photon energies. To our knowledge there is no other experimental or theoretical report of the geometries or electronic structures of the ground and excited states of Al_3O_2, $Al_3O_2^-$, Al_3O_3, or $Al_3O_3^-$. To understand the features in the recently reported photoelectron spectra of $Al_3O_2^-$ and $Al_3O_3^-$ one should have correct geometries of these species in their ground and thermally accessible excited states as well as reliable theoretical results for many electronic states of neutral Al_3O_2 and Al_3O_3. In this work, we found the ground-state geometries of neutral and anionic forms of Al_3O_2 and Al_3O_3 and electronic structures and energies of the low lying excited

* Corresponding author.
[†] On leave from Chemistry Division, Bhabha Atomic Research Centre, Trombay, Bombay 400085, India.

10.1021/jp9925839 CCC: $18.00 © 1999 American Chemical Society
Published on Web 10/21/1999

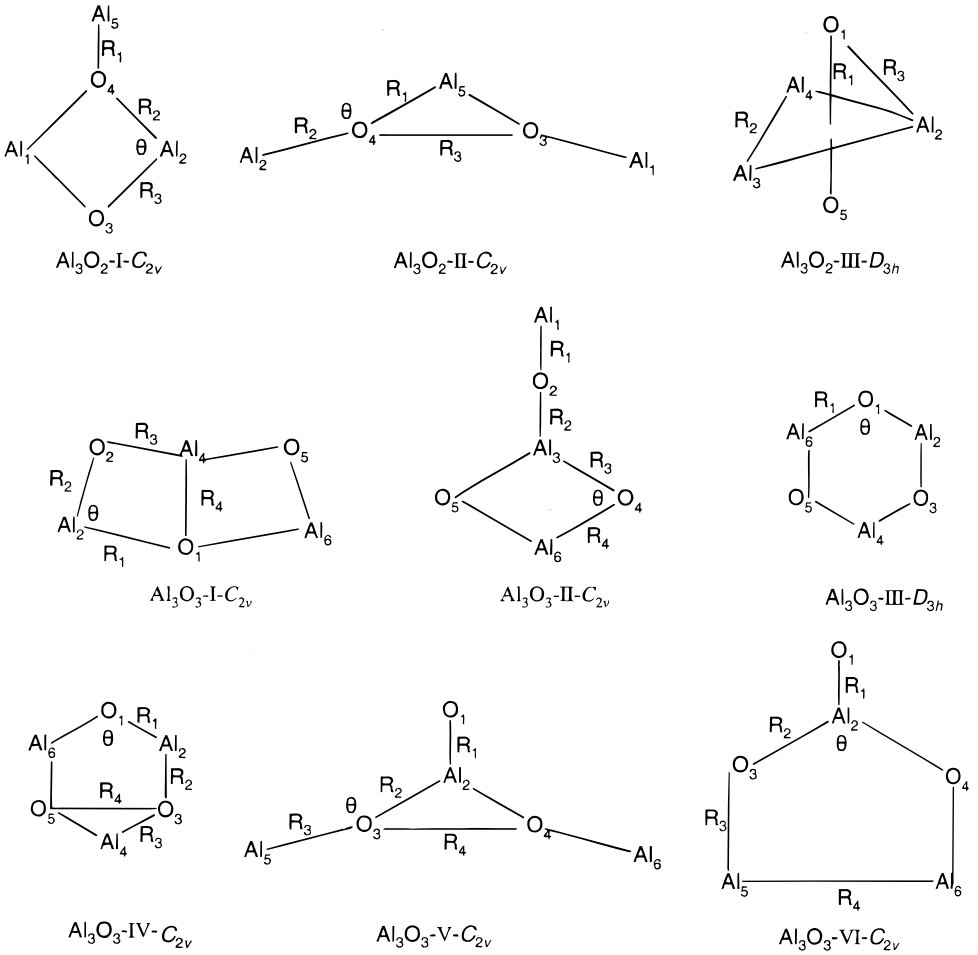

Figure 1. Structures of Al_3O_2 and Al_3O_3 investigated in this work.

states of Al_3O_2 and Al_3O_3 in order to interpret the experimentally observed photoelectron spectra of $Al_3O_2^-$ and $Al_3O_3^-$.

Theoretical Details

Hartree−Fock (HF) and density functional theoretical (DFT) calculations were performed to optimize the geometries of Al_3O_2, $Al_3O_2^-$, Al_3O_3, and $Al_3O_3^-$. The functional used in the DFT calculations was the Becke three-parameter exchange and Lee−Yang−Parr correlation (B3LYP). All the HF and DFT calculations were done using the Gaussian 98[23] program. The basis sets used for Al and O were the Dunning aug-cc-pTVZ sets excluding the f function and augmenting d function.[24] The grid for DFT had 75 radial points and 302 angular points. All orbital energies were negative for the anions. Tests of the grid for $Al_3O_3^-$ indicated the energy error due to this grid was 0.00001 hartrees. Harmonic vibrational frequencies were computed by analytic second derivative methods with HF and B3LYP, and the stationary points on the potential energy surfaces of neutral and anions of Al_3O_2 and Al_3O_3 were confirmed to be minima. Using the MELD[25] program, CI calculations were performed to calculate the ground-state wave function of the anion and vertical excited states of the neutral species at the B3LYP geometries of the anions. The starting orbitals for CI wave functions were obtained from ground-state $Al_3O_2^-$ and $Al_3O_3^-$ restricted open-shell Hartree−Fock (ROHF) computations. The virtual orbitals obtained from the ROHF calculations were converted to frozen average natural orbitals[26] to carry out the CI calculations. The 1s, 2s, and 2p electrons of aluminum and 1s electrons of oxygen were kept frozen as the core, and the remaining valence electrons were treated explicitly in the CI calculations. For the calculations on Al_3O_3, the 2s electrons of oxygen were also kept frozen as the core so that the CI calculations still would be computationally affordable.

In the frozen orbital or Koopmans' approximation, the HF orbitals from the ground state of a molecule are generally used to form Slater determinants for describing the ground or excited states of the ion. Koopmans' theorem assumes that individual Slater determinants formed by omitting one orbital from the ground state HF determinant are good approximations to the actual states of the ion. However, photoelectron spectroscopy and electron momentum spectroscopy clearly show extra structure, or so-called satellites, in the experimental binding energy spectra, which is not expected within the Koopmans' theorem picture. In other words, experimental evidence points to a breakdown of the independent-particle (frozen orbital) picture of electronic structure. There can also be excitations followed by ionization, like 1p-2h (one particle-two holes), 2p-3h (two particles-three holes), etc. Therefore, the ground state of the neutral, $\Psi(N)$, and each state of the ion, $\Psi_f(N-1)$, are written as linear combinations of all possible configurations, and this is referred to as the configuration interaction picture. This interaction among all possible configurations (allowed by symmetry) leads to a redistribution of the photoelectron peak intensity among many states of the same symmetry. Experimentally, this mixing redistributes intensity between primary hole peaks associated with primary hole states and satellite peaks associated with correlation states. The pole strength for the *f*th ionic state is defined as

$$S_f^2 = ||\langle \Psi_f(N-1)|\Psi_f(N)\rangle_{N-1}||^2$$

where the integration is performed over $N - 1$ electrons. The pole strength of the peak corresponding to the 0p-1h (primary peak) ionic state configuration will be close to unity and the pole strengths of the peaks associated with other configurations (1p-2h, 2p-3h, etc.) are usually very small ($S_f^2 \ll 1$). The photoelectron peak intensities are proportional to the pole strength multiplied by the squares of transition moments between the bound orbital and the continuum.

Results

A. Structure and Energetics. The optimized structures of the neutral and anionic species of Al_3O_2 and Al_3O_3 are sketched in Figure 1. The optimized geometrical parameters for different structures are listed in Table 1 and energies are listed in Table 2. For all the structures reported in Figure 1, harmonic vibrational frequencies were calculated to establish the nature of the stationary points. The frequencies for the lowest energy structures are listed in Table 3 and Table 4 for Al_3O_2 and Al_3O_3 species, respectively. The calculated zero-point energies are also listed in Table 2 but have not been added to the energy differences because (a) the effect is very small and (b) the unscaled zero-point energies are not a reliable estimate of the true zero point. The highest UHF frequency for structure I for both Al_3O_2 and Al_3O_3 was nearly 2000 cm^{-1} compared to a maximum frequency 1000 cm^{-1} for all other structures by all methods. This high value is unreasonable and leads to unusually large estimates of the zero-point energy. The values of $\langle S^2\rangle$ for these UHF wave functions were 0.82 and 0.91, respectively, compared with values near 0.75 for most other doublet states.

Al_3O_2 and $Al_3O_2^-$. The results in Table 2 indicate that the $^2A_1$ state of structure II (depicted as Al_3O_2-II-C_{2v} in Figure 1) is the global minimum of Al_3O_2. The energy difference between this structure ("vee" shaped) and the structure I ("kite" shaped) has been found to be 30.0 and 12.2 kcal/mol by HF and B3LYP methods. For $Al_3O_2^-$, in addition to the structure I and structure II, structure III with trigonal bipyramid shape and D_{3h} symmetry (depicted in Figure 1 as Al_3O_2-D_{3h}-III) is also found to be a minimum on the singlet potential energy surface with an $^1A_1'$ configuration. The global minimum on the $Al_3O_2^-$ potential energy surface is found to be structure II with only a marginally lower energy than structure I. At the B3LYP level, this structure II lies 0.4 kcal/mol below structure I and 22.8 kcal/mol below structure III. So structure II is the global minimum for both Al_3O_2 and $Al_3O_2^-$ as predicted by both HF and B3LYP methods. On the triplet surface, no state was found to be close in energy to the singlet states. Also, no neutral Al_3O_2 has been found to be minimum with the trigonal bipyramid shape. According to our calculation, the valence electron configurations of $Al_3O_2^-$ are . . . $(4b_1)^2(14a_1)^2(15a_1)^2(8b_2)^2$, . . . $(9b_2)^2(12a_1)^2(10b_2)^2(13a_1)^2$, and . . . $(4a_2'')^2(7a_1')^2(6e')^4$ for structure I, structure II, and structure III, respectively. At this point it is clear that for $Al_3O_2^-$ the relative energy ordering is $^1A_1(a_1^2)$ [II-C_{2v}] $\lesssim$ $^1A_1$-(b_2^2) [I-C_{2v}] < $^1A_1'$ (e'^4) [III-D_{3h}] at both the HF and B3LYP levels of theory.

Molecular orbital energy diagrams for the three lowest energy structures are reported in Figure 2. The MO diagram agrees with the view that $Al_3O_2^-$ is best regarded as an ionic cluster $(Al^{1+})_3(O^{2-})_2$. The three highest occupied MOs are primarily Al 3s in character.

Al_3O_3 and $Al_3O_3^-$. The lowest energy structure for neutral Al_3O_3 computed at the HF level is a hexagonal structure (IV-C_{2v}, $^2B_2$). The geometrical parameters for this structure are very close to the D_{3h} symmetry hexagonal structure (III-D_{3h}) with $(e')^3$ configuration, $^2E'$ state. The energy difference between these two structures is essentially zero. This $^2E'$ state is subject to Jahn−Teller distortion and $^2A_1$ and $^2B_2$ components are obtained. Unfortunately, at D_{3h}, the UHF energy for $^2B_2$ is already lower than $^2A_1$ by 56 kcal/mol, so a meaningful study of the Jahn−Teller distortion is not possible. We have found two more structures of Al_3O_3 (I-C_{2v}, $^2B_2$, "rectangle" and II-C_{2v}, $^2A_1$, "kite") which are completely different from each other and also different from the hexagon structure as depicted in Figure 1. I-C_{2v}, $^2B_2$ state and II-C_{2v}, $^2A_1$ state are 32.18 and 0.07 kcal/mol higher in energy than the most stable IV-C_{2v}, $^2B_2$ structure. We have also been able to find one more structure (V-C_{2v}, $^2B_2$) which is 19.93 kcal/mol higher in energy than the most stable structure. As already mentioned, all the geometrical parameters are presented in Table 1 and all the energy values are reported in Table 2 for all of these structures. While at the HF level, the hexagonal structure is the most stable for Al_3O_3, with B3LYP, the II-C_{2v} structure is found to be the global minimum structure. At D_{3h}, the B3LYP energy for $^2B_2$ is already below that for $^2A_1$ by 9 kcal/mol, so a meaningful study of the Jahn−Teller distortion is not possible with B3LYP either. Also, the results for both III and IV must be viewed with great caution because $\langle S^2\rangle$ exceeded 1.5 for this doublet state with both UB3LYP and UHF. Among all the structures reported in this paper, this was the only case where $\langle S^2\rangle$ computed treating the Kohn−Sham determinant as if it were actually a wave function gave a value more than 0.01 different from $M(M + 1)$.

TABLE 1: Geometries (Å, deg) of Al_3O_2, $Al_3O_2^-$, Al_3O_3, and $Al_3O_3^-$ Computed at the HF and B3LYP Levels

method	structure	state	R_1	R_2	R_3	R_4	q
			Al_3O_2				
HF	I-C_{2v}	$^2B_2$	1.752	1.898	1.717		86.7
	II-C_{2v}	$^2A_1$	1.688	1.691	2.944		179.3
B3LYP	I-C_{2v}	$^2B_2$	1.773	1.935	1.749		86.9
	II-C_{2v}	$^2A_1$	1.715	1.717	3.009		178.6
			$Al_3O_2^-$				
HF	I-C_{2v}	$^1A_1$	1.692	1.983	1.733		84.0
	II-C_{2v}	$^1A_1$	1.776	1.651	2.770		176.7
	III-D_{3h}	$^1A_1'$	1.132	2.658	1.907		
B3LYP	I-C_{2v}	$^1A_1$	1.712	2.035	1.764		84.3
	II-C_{2v}	$^1A_1$	1.812	1.679	2.817		176.3
	III-D_{3h}	$^1A_1'$	1.167	2.691	1.833		
			Al_3O_3				
HF	I-C_{2v}	$^2B_2$	1.837	1.770	1.671	1.833	88.5
	II-C_{2v}	$^2A_1$	1.697	1.663	1.722	1.730	88.2
	III-D_{3h}	$^2E'$	1.702				126.9
	IV-C_{2v}	$^2B_2$	1.702	1.703	1.702	2.846	127.2
	IV-C_{2v}	$^2A_1$	1.711	1.690	1.711	2.814	119.2
	V-C_{2v}	$^2B_2$	1.734	1.671	1.694	2.978	178.2
B3LYP	I-C_{2v}	$^2B_2$	1.883	1.805	1.697	1.860	88.8
	II-C_{2v}	$^2A_1$	1.723	1.685	1.753	1.763	87.1
	III-D_{3h}	$^2E'$	1.731				124.1
	IV-C_{2v}	$^2B_2$	1.728	1.738	1.726	2.966	126.6
	IV-C_{2v}	$^2A_1$	1.738	1.715	1.748	2.892	118.2
	V-C_{2v}	$^2B_2$	1.749	1.694	1.720	3.022	177.7
			$Al_3O_3^-$				
HF	I-C_{2v}	$^1A_1$	1.920	1.844	1.663	1.753	84.7
	II-C_{2v}	$^1A_1$	1.667	1.700	1.686	1.836	88.8
	IV-C_{2v}	$^3B_2$	1.788	1.671	1.711	2.948	102.0
	V-C_{2v}	$^1A_1$	1.618	1.740	1.651	2.786	168.6
	VI-C_{2v}	$^3B_2$	1.614	1.764	1.676	2.640	102.4
B3LYP	I-C_{2v}	$^1A_1$	1.946	1.875	1.696	1.791	85.6
	II-C_{2v}	$^1A_1$	1.690	1.730	1.718	1.867	87.9
	III-D_{3h}	$^3A_2'$	1.748				125.5
	V-C_{2v}	$^1A_1$	1.645	1.766	1.677	2.809	170.9
	VI-C_{2v}	$^3B_2$	1.673	1.751	1.735	2.822	110.2

TABLE 2: Calculated Energies[a] of Low Lying Electronic States of Al_3O_2, $Al_3O_2^-$, Al_3O_3, and $Al_3O_3^-$

method	structure (state)	energy (E_h)	ΔE[a] (kcal/mol)	zpe[b] (kcal/mol)
		Al_3O_2		
HF	I-C_{2v} ($^2B_2$)	−875.706961	0.00	7.88
	II-C_{2v} ($^2A_1$)	−875.754864	−30.06	5.80
B3LYP	I-C_{2v} ($^2B_2$)	−878.027165	0.0	5.00
	II-C_{2v} ($^2A_1$)	−878.046671	−12.24	5.23
		$Al_3O_2^-$		
HF	I-C_{2v} ($^1A_1$)	−875.763585	0.00	5.51
	II-C_{2v} ($^1A_1$)	−875.764182	−0.37	5.42
	III-D_{3h} ($^1A_1'$)	−875.713303	31.55	5.44
B3LYP	I-C_{2v} ($^1A_1$)	−878.099760	0.00	4.85
	II-C_{2v} ($^1A_1$)	−878.100388	−0.39	4.88
	III-D_{3h} ($^1A_1'$)	−878.063394	22.82	4.81
		Al_3O_3		
HF	I-C_{2v} ($^2B_2$)	−950.662663	0.0	10.14
	II-C_{2v} ($^2A_1$)	−950.713834	−32.11	9.21
	III-D_{3h} ($^2E'$)	−950.713942	−32.18	9.28
	IV-C_{2v} ($^2B_2$)	−950.713947	−32.18	9.28
	IV-C_{2v} ($^2A_1$)	−950.625979	23.02	8.38
	V-C_{2v} ($^2B_2$)	−950.682189	−12.25	7.75
B3LYP	I-C_{2v} ($^2B_2$)	−953.353072	0.0	8.04
	II-C_{2v} ($^2A_1$)	−953.370766	−11.10	8.33
	III-D_{3h} ($^2E'$)	−953.346511	4.12	8.26
	IV-C_{2v} ($^2B_2$)	−953.346755	3.96	8.25
	IV-C_{2v} ($^2A_1$)	−953.332547	12.88	7.93
	V-C_{2v} ($^2B_2$)	−953.310987	26.41	7.06
		$Al_3O_3^-$		
HF	I-C_{2v} ($^1A_1$; b_2^2)	−950.739870	0.00	8.86
	II-C_{2v} ($^1A_1$; a_1^2)	−950.744349	2.81	8.68
	IV-C_{2v} ($^3B_2$; $b_2^1a_1^1$)	−950.728225	7.31	8.62
	V-C_{2v} ($^1A_1$; b_2^2)	−950.708343	19.78	8.00
	VI-C_{2v} ($^3B_2$; $b_2^1a_1^1$)	−950.637593	64.17	8.63
B3LYP	I-C_{2v} ($^1A_1$; b_2^2)	−953.449225	0.00	7.93
	II-C_{2v} ($^1A_1$; a_1^2)	−953.447835	0.87	7.83
	III-D_{3h} ($^3A_2'$; e'^2)	−953.423712	16.01	7.55
	V-C_{2v} ($^1A_1$; b_2^2)	−953.414804	21.60	7.32
	VI-C_{2v} ($^3B_2$; $b_2^1a_1^1$)	−953.336373	70.81	7.26

[a] For each method, the energy difference was calculated relative to the $^2B_2$ and $^1A_1$ energies of the neutral and negative ion respectively for Al_3O_2 and Al_3O_3 species. [b] Calculated zero-point energies.

The large $\langle S^2 \rangle$ and the possibility of a Jahn−Teller distortion indicate that there might be a strong multiconfiguration effect on the structures and energies of Al_3O_3. To test this possibility, we have optimized the four structures using a small three-electron/three-orbital CASSCF/6-31G* wave function, followed by single-point CASMP2 calculations. Using the HONDO[27] program, it has been found that II is more stable than the IV by 11.00 and 10.36 kcal/mol, respectively. Therefore, on the basis of the present B3LYP and CASMP2 results, the ground-state geometry of the Al_3O_3 molecule is the II-C_{2v} ($^2A_1$) isomer.

According to the present HF calculations, the lowest state of $Al_3O_3^-$ is I-C_{2v} (b_2^2, $^1A_1$) and the next lowest state II-C_{2v} (a_1^2, $^1A_1$) is found to be at 2.81 kcal/mol higher in energy. We have also found three more minimum energy isomers on the ground-state potential energy surface of $Al_3O_3^-$, viz., IV-C_{2v} ($^3B_2$), V-C_{2v} ($^1A_1$), and VI-C_{2v} ($^3B_2$) which lie at 10.12, 22.59, and 66.96 kcal/mol high in energy. Similarly, the B3LYP method predicts I-C_{2v} ($^1A_1$) as the global minimum structure among all the $Al_3O_3^-$ isomers considered here, but it is only 0.87 kcal/mol more stable than the next minimum energy isomer II-C_{2v} ($^1A_1$). On the triplet surface, the III-D_{3h} structure with D_{3h} symmetry is found to be minimum. This is 16.01 kcal/mol higher in energy than the lowest energy state. The valence electron configurations have been found to be I-C_{2v} ($^1A_1$), . . . $(14a_1)^2$-$(2a_2)^2(4b_1)^2(15a_1)^2(11b_2)^2$, II-$C_{2v}$ ($^1A_1$) . . . $(5b_1)^2(8b_2)^2(1a_2)^2$-$(17a_1)^2(18a_1)^2$, and III-D_{3h} ($^3A_2'$) . . . $(8e')^4(2e'')^4(9e')^2(7a_1')^2$. Figure 3 shows the orbital energies and labels for $Al_3O_3^-$ for the three lowest energy isomers. The bonding in $Al_3O_3^-$ is roughly $Al^{3+}(Al^{1+})_2(O^{2-})_3$ with the Al^{3+} ion surrounded by three neighboring O^{2-} ions. Like the $Al_3O_2^-$ structures, the Al^{1+} ions tend to have only one or two O^{2-} neighbors. In agreement with this conceptual assignment, only two of the MOs in Figure 3 are of Al 3s type.

TABLE 3: Calculated Harmonic Vibrational Frequencies (in cm^{-1}) and Infrared Intensities of Low-Energy Isomers of Al_3O_2 and $Al_3O_2^-$ by the B3LYP Method

Al_3O_2 I-C_{2v} ($^2B_2$)		Al_3O_2 II-C_{2v} ($^2A_1$)	
symmetry	frequency	symmetry	frequency
a_1	789.9 (156.7)	b_2	1006.1 (937.5)
a_1	714.5 (261.6)	a_1	986.3 (153.3)
b_2	661.6 (92.7)	b_2	565.3 (9.0)
a_1	417.2 (44.1)	a_1	450.1 (11.4)
a_1	332.4 (3.4)	a_1	247.5 (28.8)
b_1	226.9 (1.5)	b_1	132.9 (5.3)
b_2	164.1 (134.7)	a_2	118.6 (0.0)
b_1	104.5 (1.6)	b_2	106.3 (1.0)
b_2	88.1 (3.9)	a_1	46.2 (0.1)
$Al_3O_2^-$ I-C_{2v} ($^1A_1$)		$Al_3O_2^-$ II-C_{2v} ($^1A_1$)	
symmetry	frequency	symmetry	frequency
a_1	838.4 (234.5)	a_1	973.2 (290.5)
b_2	737.7 (343.8)	b_2	951.3 (699.0)
a_1	673.6 (70.1)	b_2	452.8 (40.0)
a_1	355.6 (33.2)	a_1	429.8 (60.7)
a_1	265.7 (9.1)	a_1	245.7 (10.5)
b_2	192.1 (113.1)	b_1	115.7 (3.6)
b_1	180.6 (9.3)	a_2	104.1 (0.0)
b_1	90.6 (0.1)	b_2	94.6 (0.3)
b_2	59.6 (0.3)	a_1	45.1 (0.9)

B. Photoelectron Spectra. *$Al_3O_2^-$*. Since no experimental or theoretical structures are available for Al_3O_2 or $Al_3O_2^-$, we have decided to rely on the present optimized B3LYP structures to calculate the vertical excited states of Al_3O_2. Although structure II of $Al_3O_2^-$ is slightly lower in energy than structure I (by 0.4 kcal/mol), from the orbital energy diagram in Figure 2 it is clear that structure II has a higher HOMO energy than structure I. The experimental photoelectron spectrum (PES) of $Al_3O_2^-$ can be rationalized if it is considered that, due to the higher HOMO energy (−1.83 eV), structure II can be easily ionized to produce an X′ peak (1.90 eV). On the other hand, structure I has a lower HOMO energy (−2.42 eV) and it can account for the X peak (2.29 eV). On the basis of these facts, we have assumed both structure I and structure II contribute to the PES of $Al_3O_2^-$. Structure III is energetically much higher than either structure I or structure II, so according to the Boltzman distribution it is unlikely to have sufficient fraction of this isomer (in the equilibrium mixture) to contribute anything to PES. Hence only the vertical transitions from the I-C_{2v}-$^1A_1$ (b_2^2) and II-C_{2v}-$^1A_1$ (a_1^2) isomers of $Al_3O_2^-$ to the various states of neutral Al_3O_2 have been considered. We have reported the results of 2h-1p CI calculations for different excited states of Al_3O_2 obtained at I-C_{2v}-$^1A_1$ and II-C_{2v}-$^1A_1$ anion geometries in Figure 4a. In this figure, the energy of all roots from structure I-C_{2v}-$^1A_1$ (b_2^2) have been shifted by a constant so that the lowest energy root ($^2B_2$) agrees with the corresponding 2.29 eV experimental vertical ionization peak (X). Similarly, for the structure II-C_{2v}-$^1A_1$ (a_1^2), the energy of all roots has been shifted by a constant so that the lowest energy root ($^2A_1$) agrees with the corresponding 1.90 eV experimental peak (X′). It is to be noted that if one considers only one isomer of $Al_3O_2^-$, all the features in the experimental spectrum cannot be explained. For

TABLE 4: Calculated Harmonic Vibrational Frequencies (in cm^{-1}) and Infrared Intensities of Low-Energy Isomers of Al_3O_3 and $Al_3O_3^-$ by the B3LYP Method

Al_3O_3 I-C_{2v} ($^2B_2$)		Al_3O_3 II-C_{2v} ($^2A_1$)		Al_3O_3 IV-C_{2v} ($^2B_2$)		$Al_3O_3^-$ I−C_{2v} ($^1A_1$)		$Al_3O_3^-$ II−C_{2v} ($^1A_1$)	
symmetry	frequency	symmetry	frequency	symmetry	frequency	symmetry	frequency	symmetry	frequency
b_2	981.1 (0.3)	a_1	1066.8 (706.9)	b_2	886.9 (276.8)	b_2	995.6 (202.5)	a_1	1043.4 (808.9)
a_1	725.7 (14.3)	a_1	797.7 (0.6)	b_2	867.2 (9.5)	a_1	737.9 (4.6)	a_1	839.7 (7.9)
a_1	636.4 (183.8)	b_2	757.7 (200.4)	a_1	830.5 (76.1)	a_1	679.8 (74.4)	b_2	813.9 (109.1)
a_1	571.0 (25.5)	a_1	742.3 (199.6)	b_2	659.5 (21.6)	b_2	570.8 (285.6)	a_1	591.3 (95.9)
b_2	565.5 (135.8)	b_2	632.7 (2.0)	a_1	648.3 (41.6)	a_1	532.4 (159.2)	a_1	538.7 (78.6)
b_2	554.6 (184.7)	a_1	585.1 (50.2)	a_1	567.9 (0.2)	b_2	455.1 (3.2)	b_2	483.1 (68.8)
a_1	430.8 (0.1)	b_1	356.9 (80.9)	a_1	401.9 (0.3)	a_1	412.4 (0.6)	b_1	333.9 (29.9)
b_1	333.7 (42.3)	a_1	341.3 (9.3)	b_2	234.0 (22.5)	b_2	354.4 (121.9)	a_1	323.4 (2.1)
b_2	296.8 (296.8)	b_2	238.6 (11.5)	b_1	213.8 (19.1)	b_1	331.5 (17.1)	b_2	232.1 (5.0)
a_1	244.7 (1.9)	b_1	177.7 (1.2)	a_1	205.9 (8.8)	a_1	206.1 (1.8)	b_1	155.0 (7.2)
a_2	175.7 (0.0)	b_1	69.2 (0.4)	a_2	132.9 (0.0)	a_2	161.3 (0.0)	b_1	64.1 (4.3)
b_1	104.9 (7.5)	b_2	60.8 (0.8)	b_1	123.0 (0.0)	b_1	106.9 (19.8)	b_2	56.3 (0.6)

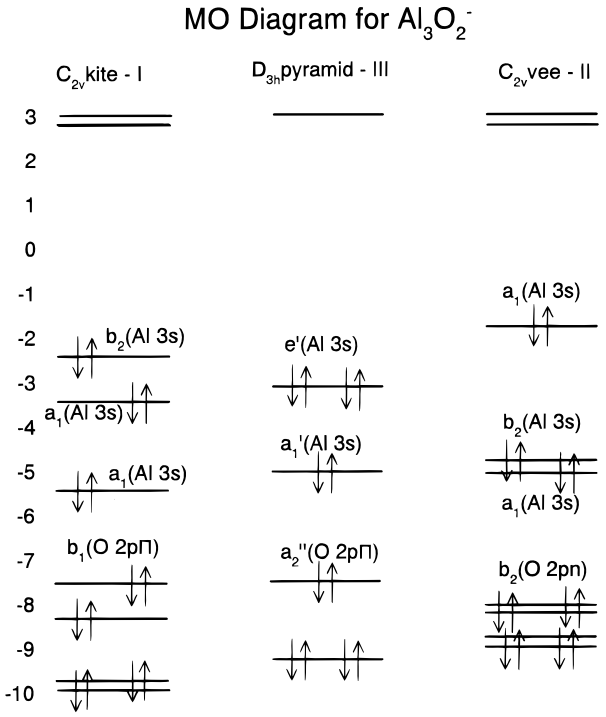

Figure 2. Orbital energy (eV) diagram for $Al_3O_2^-$ $(8b_2)^2\ ^1A_1$, $(6e')^4\ ^1A_1'$, and $(13a_1)^2\ ^1A_1$ states.

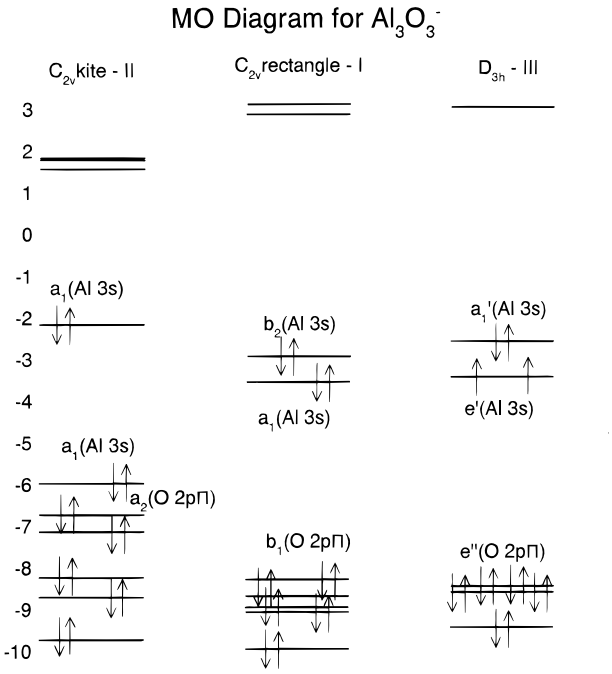

Figure 3. Orbital energy (eV) diagram for $Al_3O_3^-$ $(18a_1)^2\ ^1A_1$, $(11b_2)^2\ ^1A_1$, and $(9e')^2\ ^3A_2'$ states.

both shapes of the negative ion of Al_3O_2, small CI calculations have been performed and, for each negative ion geometry using the negative ion wave function and corresponding neutral wave functions, pole strength values have been calculated for different states. Starting with each structure, for each symmetry the lowest 20 roots are considered and only those states whose calculated pole strength values are greater than 0.01 have been considered. Gaussians of fixed width with heights proportional to the pole strength scaled to match the first two peaks have been used to construct the simulated spectrum. In this construction shown in Figure 4b the energy separation from the first A_1 or B_2 peak was also scaled to best simulate the next peaks in the spectrum.

To get more accurate excited state energy values and wave functions, MRSDCI calculations have been performed for the lowest few roots of the CI matrix of each symmetry to cover the range of binding energies of approximately 8 eV. This has been done separately starting from each of the low-energy isomers of $Al_3O_2^-$. For each symmetry, the dominant configurations from the 2h-1p CI calculations with coefficients greater than 0.05 were used to construct the reference space, and perturbation theory was used to select approximately 500 000−800 000 configurations for each symmetry. Similarly for the negative ions of Al_3O_2, MRSDCI calculations were performed to get the ground-state wave function for computing the Dyson orbitals and the corresponding pole strength. The calculated ground-state energies were $-876.2416499E_h$ and $-876.2621979E_h$ for the C_{2v}-I-$^1A_1$ and C_{2v}-II-$^1A_1$ states, respectively. In Table 5, we have reported the results of MRSDCI calculations for different excited states of Al_3O_2 starting from both the states, $^1A_1$ (a_1^2) and $^1A_1$ (b_2^2). Similar to the case of 2h-1p calculations, here also the energy of all roots obtained from structure I and structure II has been shifted by constants so that the respective two lowest energy roots agree with the corresponding 2.29 and 1.90 eV vertical ionization peaks in the experimental spectrum. In addition to the binding energies, Table 5 also includes the calculated pole strength values (S_f^2), and the leading terms in the wave function for each state. From Table 5, the primary hole states can be easily identified since the CI coefficients for these configurations are close to unity.

Theoretically calculated binding energy spectra of $Al_3O_2^-$ using the 2h-1p and MRSDCI results obtained in the present work have been reported in Figures 4 and 5, respectively. As mentioned above, the position and the intensities of the first peak from both the transitions from $^1A_1(a_1^2)$ and $^1A_1(b_2^2)$ state of $Al_3O_2^-$ to neutral Al_3O_2 have been matched with 1.90 and

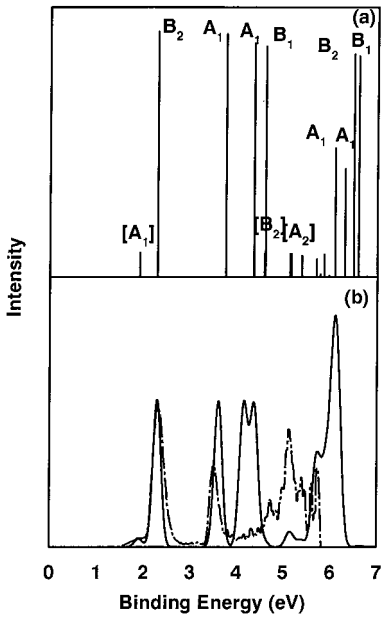

Figure 4. (a) Theoretical spectrum obtained using the calculated energies and pole strength values from 2h−1p calculations for $Al_3O_2^-$. The peaks have been shifted and scaled to make the first two peaks agree with experiment. (b) Comparison between the experimentally observed and theoretically derived photoelectron spectrum of $Al_3O_2^-$. The dashed line represents the experimental spectrum and solid line represents the theoretical simulated spectrum.

2.29 eV experimental peaks, respectively, and all other peak positions and intensities for the two sets of transitions are shifted accordingly to derive the theoretical spectrum in part A of the figures. In part B, the separation of the higher peaks from the lowest one of each symmetry is uniformly scaled. Qualitatively, both of the calculated spectra (Figures 4 and 5) are similar. The photoelectron peaks corresponding to the transitions from $^1A_1$-(a_1^2) of $Al_3O_2^-$ are indicated within the square brackets in Figures 4a and 5a. For the purpose of comparison, the experimental spectrum is plotted in Figures 4b and 5b as a dashed line. It is clear from Figures 4 and 5 that the MRSDCI calculated spectrum agrees better with the experimental one than the 2h-1p calculated spectrum.

Although in the smoothed spectrum the very low intensity features are not clear due to the Gaussian fitting, the calculated line spectrum of Figures 4a and 5a show some of these features. The present theoretical results suggest that there are two electronic states of the negative ion of Al_3O_2 (from two different structures) involved in the photoelectron spectrum. In the observed experimental spectrum of $Al_3O_2^-$, no symmetry assignment was made by Wu et al.[22] On the basis of the present calculated results and the assumptions outlined above, we have provided assignments for the different peaks observed in the experimental spectrum and have represented them in Figures 4 and 5. The very first low intensity peak (X′) is assigned as $(13a_1)^{-1}\ ^2A_1 \leftarrow {}^1A_1(a_1^2)$. The second peak (X(3s)) is due to the $(8b_2)^{-1}\ ^2B_2 \leftarrow {}^1A_1\ (b_2^2)$ transition. The third peak which was denoted by Wu et al. as A(3s), has been found to be $(15a_1)^{-1}$ $^2A_1 \leftarrow {}^1A_1\ (b_2^2)$. Some low intensity satellite structures between the third and fourth peak are due to the $(10b_2)^{-1}\ ^2B_2 \leftarrow {}^1A_1$-$(a_1^2)$ and $(12a_1)^{-1}\ ^2A_1 \leftarrow {}^1A_1(a_1^2)$ transitions. The fourth low intensity peak (represented as B(3s)) has been found to be due to the low intensity primary hole $(14a_1)^{-1}\ ^2A_1 \leftarrow {}^1A_1\ (b_2^2)$ transition mixed with 2h-1p transitions. The last peak (represented as C (O 2p)) has been assigned to two transitions, $(14a_1)^{-1}\ ^2A_1 \leftarrow {}^1A_1\ (b_2^2)$ and $(4b_1)^{-1}\ ^2B_1 \leftarrow {}^1A_1\ (b_2^2)$.

TABLE 5: Calculated[a] Line Positions and Intensities for the Photoelectron Spectrum of $Al_3O_2^-$ with the Transitions from $^1A_1\ (b_2^2)$ and $^1A_1\ (a_1^2)$ States of $Al_3O_2^-$ (C_{2v}) Being Considered

state	binding energy[b] (eV)	intensity[c] (S_j^2)	important configurations[d]
		$Al_3O_2^-$ ($^1A_1\ (b_2^2)$ C_{2v})	
$^2B_2$	2.29	0.93	$0.91(8b_2)^{-1}$
$^2A_1$	3.52	0.94	$0.91(15a_1)^{-1}$
$^2A_1$	5.62	0.14	$0.76(14a_1)^{-1}\ (8b_2)^{-1}\ (9b_2)^1$
			$0.36(15a_1)^{-1}\ (8b_2)^{-1}\ (9b_2)^1$
			$0.35(14a_1)^{-1}$
$^2A_1$	5.85	0.79	$0.80(14a_1)^{-1}$
			$0.33(14a_1)^{-1}\ (8b_2)^{-1}\ (9b_2)^1$
			$0.25(13a_1)^{-1}$
$^2B_1$	6.30	0.86	$0.88(4b_1)^{-1}$
$^2A_1$	7.18	0.89	$0.85(13a_1)^{-1}$; $0.28(14a_1)^{-1}$
$^2B_2$	7.90	0.02	$0.91(15a_1)^{-1}(16a_1)\ ^1(8b_2)^{-1}$
			$0.41(8b_2)^{-2}(10b_2)^1$
			$0.41(8b_2)^{-2}(9b_2)^1$
			$0.31(14a_1)^{-1}(15a_1)\ ^1(9b_2)^{-1}$
$^2B_2$	8.64	0.76	$0.83(7b_2)^{-1}$; $(8b_2)^{-2}\ (10b_2)^1$
		$Al_3O_2^-$ ($^1A_1\ (a_1^2)$ C_{2v})	
$^2A_1$	1.90	0.94	$0.91(13a_1)^{-1}$
$^2B_2$	5.13	0.91	$0.90(10b_2)^{-1}$
$^2A_1$	5.35	0.85	$0.87(12a_1)^{-1}$
$^2A_1$	5.95	0.07	$0.64(12a_1)^{-1}(13a_1)^{-1}(14a_1)\ ^1$
			$0.56(13a_1)^{-1}(10b_2)^{-1}(11b_2)^1$
			$0.26(12a_1)^{-1}$
$^2B_2$	5.95	0.03	$0.70(13a_1)^{-1}(14a_1)\ ^1(10b_2)^{-1}$
			$0.52(12a_1)^{-1}(13a_1)\ ^1(11b_2)^1$
$^2B_1$	5.98	0.01	$0.81(4b_1)^1(13a_1)^{-1}$
			$0.29(13a_1)^{-1}(10b_2)^{-1}(3a_2)^{-1}$
			$0.27(12a_1)^{-1}(13a_1)^{-1}(5b_1)^1$
$^2B_2$	7.00	0.89	$0.90(9b_2)^{-1}$
$^2A_2$	7.28	0.89	$0.90(2a_2)^{-1}$
$^2A_1$	7.80	0.88	$0.90(11a_1)^{-1}$
$^2B_1$	8.01	0.10	$0.82(12a_1)^{-1}(13a_1)^{-1}(4b_1)^1$
			$0.31(3b_1)^{-1}$
$^2B_1$	8.21	0.50	$0.68(3b_1)^{-1}$
			$0.44(13a_1)^{-1}(10b_2)^{-1}(3a_2)^1$
			$0.40(12a_1)^{-1}(13a_1)^{-1}(5b_1)^1$
$^2A_1$	8.37	0.03	$0.66(12a_1)^{-1}(13a_1)^{-1}(15a_1)\ ^1$
			$0.51(13a_1)^{-1}(10b_2)^{-1}(12b_2)^1$
			$0.51(13a_1)^{-1}(10b_2)^{-1}(11b_2)^1$
$^2B_2$	8.83	0.02	$0.68(13a_1)^{-1}(15a_1)\ ^1(10b_2)^{-1}$
			$0.47(12a_1)^{-1}(13a_1)^{-1}(12b_2)^1$
			$0.30(12a_1)^{-1}(13a_1)^{-1}(11b_2)^1$

[a] For each symmetry, the MRSDCI wave functions were used for the anion and neutral molecule. [b] The first $^2B_2$ state (b_2^1) and $^2A_1$ state (a_1^1) energies were adjusted to experimental data (2.29 and 1.90 eV, respectively) and the same constant shifts used for all other states. [c] The values less than 0.01 were not listed. [d] The absolute values for the CI coefficients were taken.

$Al_3O_3^-$. The optimized B3LYP geometries of $Al_3O_3^-$ from this work have been used to calculate the vertical excited states of neutral Al_3O_3, since no experimental or theoretical geometries are available in the literature. According to both the HF and B3LYP calculations, the ground state of $Al_3O_3^-$ has been found to be the bicyclic rectangle shape Al_3O_3 -I-C_{2v} (b_2^2, $^1A_1$) structure. From the MO diagram of Al_3O_3 (see Figure 3), it is clear that the HOMO orbital energy is −2.98 eV, which corresponds to the experimentally observed X(3s) peak at 2.96 eV. To explain the low intensity X′ peak in the experimental spectrum, one must consider another isomer of $Al_3O_3^-$. From the Table 2, one can see that the next lowest energy isomer of $Al_3O_3^-$ is Al_3O_3-II-C_{2v} (a_1^2, $^1A_1$) which is 0.87 kcal/mol higher in energy than the most stable isomer. Because of this low-energy difference between these two isomers it is assumed the Al_3O_3-II-C_{2v} (a_1^2, $^1A_1$) isomer is likely to be sufficiently present in the equilibrium mixture to contribute intensity in the

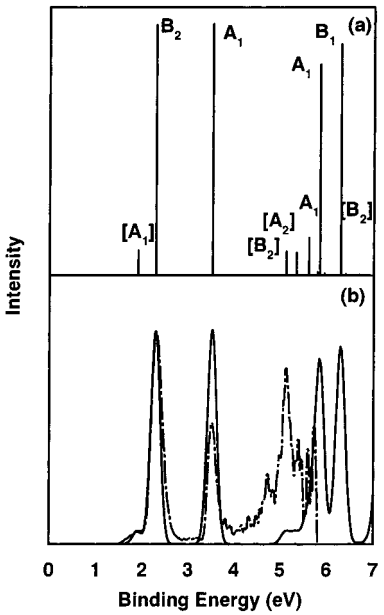

Figure 5. (a) Theoretical spectrum obtained using the calculated energies and pole strength values from MRSDCI calculations for $Al_3O_2^-$. The peaks have been shifted and scaled to make the first two peaks agree with experiment. (b) Comparison between the experimentally observed and theoretically derived photoelectron spectrum of $Al_3O_2^-$. The dashed line represents the experimental spectrum, and the solid line represents the theoretical simulated spectrum.

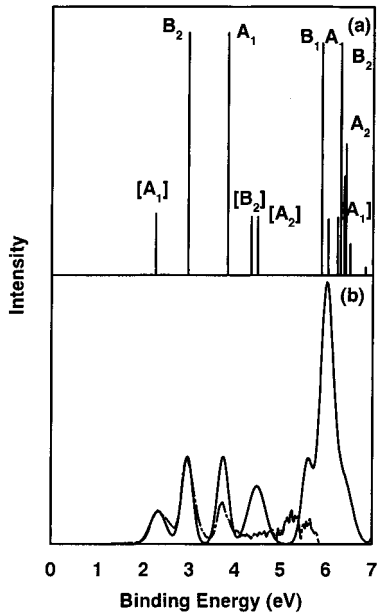

Figure 6. (a) Theoretical spectrum obtained using the calculated energies and pole strength values from 2h−1p calculations for $Al_3O_3^-$. The peaks have been shifted and scaled to make the first two peaks agree with experiment. (b) Comparison between the experimentally observed and theoretically derived photoelectron spectrum of $Al_3O_3^-$. The dashed line represents the experimental spectrum, and the solid line represents the theoretical simulated spectrum.

photoelectron spectrum of $Al_3O_3^-$. Moreover, if one considers the HOMO energy of the Al_3O_3-II-C_{2v} (a_1^2, $^1A_1$) isomer (−2.16 eV), it is possible to rationalize the X′ peak (2.25 eV) in the experimental spectrum. All other isomers of $Al_3O_3^-$ reported in Tables 1 and 2 are energetically so high that those are not likely to contribute anything in the photoelectron spectrum. On the basis of these preliminary arguments, it has been assumed that structure I and structure II together are responsible for the experimentally observed photoelectron spectrum of $Al_3O_3^-$. Vertical excited states of neutral Al_3O_3 have been calculated using both these geometries of $Al_3O_3^-$. Using each of the negative ion geometries, small CI calculations have been done to calculate the $Al_3O_3^-$ wave functions, and those were used to calculate the pole strength values. Similar to Al_3O_2, the results of 2h-1p calculations for different excited states of Al_3O_3 obtained from I-C_{2v}-$^1A_1$ and II-C_{2v}-$^1A_1$ have been reported in Figure 6. In this figure, the energies of all roots from structure I-C_{2v}-$^1A_1$ (b_2^2) have been shifted by a constant so that the lowest energy root ($^2B_2$) agrees with the corresponding 2.96 eV experimental peak (X). Similarly, for the structure II-C_{2v}-$^1A_1$ (a_1^2), the energy of all roots has been shifted by a constant so that the lowest energy root ($^2A_1$) agrees with the corresponding 2.25 eV experimental peak (X′).

The next higher level of calculation has been MRSDCI calculations for the lowest few roots in each symmetry to cover the range up to 8 eV binding energy. The dominant configurations from the 2h-1p CI calculations (coefficient greater than 0.05) were used as the reference space, and the perturbation theory was used to select approximately 500 000−800 000 configurations in each symmetry. MRSDCI calculations were also done for the negative ion at each of the geometries to calculate the pole strength values. The calculated negative ion ground states energies were $-951.243665E_h$ and $-951.249962E_h$ for the I-C_{2v}-$^1A_1$ (b_2^2) and II-C_{2v}-$^1A_1$ (a_1^2) states, respectively. In Table 6 we have presented the MRSDCI results for different excited states of $Al_3O_3^-$ obtained using each of the geometries. The energies of all roots have been shifted as discussed above for the 2h-1p case. In addition to the binding energies, we have reported the calculated pole strength values and the leading terms in the wave function for each state.

The 2h-1p and MRSDCI calculated binding energy spectrum of $Al_3O_3^-$ have been presented in Figures 6 and 7, respectively. As mentioned before, the position and intensities of the first peak obtained from both structure I and structure II of $Al_3O_3^-$ have been matched with 2.96 and 2.25 eV experimental peaks. All other binding energies are adjusted by the same amounts. The photoelectron peaks corresponding to the transitions from $^1A_1(a_1^2)$ of $Al_3O_3^-$ are indicated within the square brackets in Figures 6a and 7a. The peak positions and intensities corresponding to the line spectrum of Figures 6a and 7a have been used to generate a pseudospectrum (after uniformly scaling the energy difference from the lowest peak) and are plotted as Figures 6b and 7b, respectively. The experimental spectra are also plotted as dashed lines in the same figures. Qualitatively both the 2h-1p and MRSDCI calculated spectra are similar.

On the basis of the present 2h-1p and MRSDCI results, we have provided assignments for the different peaks in the experimental spectrum and labeled those in Figures 6 and 7. As already mentioned according to orbital energy diagram, the first low intensity peak (X′) originates from the structure-II-C_{2v}-$^1A_1$ (a_1^2) and is due to the $(18a_1)^{-1}\ ^2A_1 \leftarrow {}^1A_1(a_1^2)$ transition. The second peak (X(3s)) is assigned as the $(11b_2)^{-1}\ ^2B_2 \leftarrow {}^1A_1$ (b_2^2) transition. The third peak, which was denoted by Wu et al. as A(3s), has been found to be $(15a_1)^{-1}\ ^2A_1 \leftarrow {}^1A_1$ (b_2^2). After the third peak, the experimental spectrum is not well resolved and the next experimental peak (denoted as B(O 2p)) is most likely due to $(8b_2)^{-1}\ ^2B_2 \leftarrow {}^1A_1(a_1^2)$, $(1a_2)^{-1}\ ^2A_2 \leftarrow {}^1A_1(a_1^2)$, and $(17a_1)^{-1}\ ^2A_1 \leftarrow {}^1A_1(a_1^2)$ transitions.

Summary

Equilibrium geometries of Al_3O_2, $Al_3O_2^-$, Al_3O_3, and $Al_3O_3^-$ have been obtained by using HF and B3LYP levels of theory.

TABLE 6: Calculated[a] Line Positions and Intensities for the Photoelectron Spectrum of $Al_3O_3^-$ with the Transitions from $^1A_1$ (b_2^2) and $^1A_1$ (a_1^2) States of $Al_3O_3^-$ (C_{2v}) Being Considered

state	binding energy[b] (eV)	intensity[c] (S_j^2)	important configurations[d]
		$Al_3O_3^-$ ($^1A_1$ (b_2^2) C_{2v})	
$^2B_2$	2.96	0.94	$0.91(11b_2)^{-1}$
$^2A_1$	3.67	0.94	$0.91(15a_1)^{-1}$
$^2B_1$	7.48	0.91	$0.90(4b_1)^{-1}$
$^2B_2$	7.49	0.01	$0.90(15a_1)^{-1}(16a_1)^1(11b_2)^{-1}$
$^2A_1$	7.71	0.10	$0.71(11b_2)^{-2}(17a_1)^1$
			$0.49(15a_1)^{-2}(17a_1)^1$
			$0.29(14a_1)^{-1}$
$^2A_1$	7.81	0.04	$0.73(11b_2)^{-2}(16a_1)^1$
			$0.52(15a_1)^{-2}(16a_1)^1$
			$0.20(14a_1)^{-1}$
$^2A_1$	7.89	0.78	$0.83(14a_1)^{-1}$
			$0.23(11b_2)^{-2}(17a_1)^1$
			$0.19(15a_1)^{-2}(17a_1)^1$
$^2B_2$	7.97	0.89	$0.89(10b_2)^{-1}$
$^2A_2$	8.01	0.90	$0.90(2a_2)^{-1}$
$^2B_2$	8.35	0.02	$0.90(15a_1)^{-1}(17a_1)^1(11b_2)^{-1}$
			$0.29(11b_2)^{-2}(12b_2)^1$
			$0.17(15a_1)^{-2}(12b_2)^1$
		$Al_3O_3^-$ ($^1A_1$ (a_1^2) C_{2v})	
$^2A_1$	2.25	0.94	$0.92(18a_1)^{-1}$
$^2B_2$	5.75	0.89	$0.89(8b_2)^{-1}$
			$0.16(18a_1)^{-1}(20a_1)^1(8b_2)^{-1}$
$^2A_2$	5.85	0.89	$0.90(1a_2)^{-1}$
			$0.16(18a_1)^{-1}(20a_1)^1(1a_2)^{-1}$
$^2A_1$	6.27	0.95	$0.92(17a_1)^{-1}$
$^2B_1$	6.90	0.91	$0.76(18a_1)^{-2}(6b_1)^1$
			$0.41(5b_1)^{-1}$
			$0.30(18a_1)^{-2}(7b_1)^1$
$^2B_1$	7.48	0.71	$0.79(5b_1)^{-1}$
			$0.40(18a_1)^{-2}(6b_1)^1$
$^2B_2$	7.50	0.89	$0.89(7b_2)^{-1}$
			$0.16(18a_1)^{-1}(20a_1)^1(7b_2)^{-1}$
$^2A_1$	7.97	0.01	$0.92(17a_1)^{-1}(18a_1)^{-1}(19a_1)^{-1}$
$^2A_1$	9.02	0.87	$0.88(15a_1)^{-1}$

[a] For each symmetry, the MRSDCI wave functions were used for the anion and neutral molecule. [b] The first $^2B_2$ state (b_2^1) and $^2A_1$ state (a_1^1) energies were adjusted to experimental data (2.96 and 2.25 eV, respectively) and the same constant shifts used for all other states.[c] The values less than 0.01 were not listed. [d] The absolute values for the CI coefficients were taken.

The calculated global minima for Al_3O_2 and $Al_3O_2^-$ were found to be "vee"-shaped structures with C_{2v} symmetry. The corresponding electronic states were $^2A_1$ and $^1A_1$ with highest occupied molecular orbital occupancies $(13a_1)^1$ and $(13a_1)^2$. We have found another C_{2v} structure with a "kite" shape and the corresponding electron configurations were $(8b_2)^1$, $^2B_2$ and $(8b_2)^2$, $^1A_1$ for the neutral and negative ion, respectively. With HF and B3LYP calculations, the "kite" structure was found to be slightly higher in energy than the "vee" structure for both Al_3O_2 and $Al_3O_2^-$. The $^1A_1'$ $(e')^4$ state of $Al_3O_2^-$ was found to have D_{3h} symmetry with trigonal bipyramid shape and was much higher in energy than either of the $^1A_1$ states at their C_{2v} minima.

For $Al_3O_3^-$, the calculated global minimum was found to be a bicyclic rectangle shape with $^1A_1$ $(11b_2)^2$ electron configuration and C_{2v} symmetry, whereas the corresponding neutral Al_3O_3 with $(11b_2)^1$ $^2B_2$ configuration was found to be a local minimum. On the other hand, a "kite" shape structure with $(18a_1)^1$ $^2A_1$ state (C_{2v} symmetry) was the global minimum for Al_3O_3 and the corresponding negative ion was a local minimum. The lowest triplet state of $Al_3O_3^-$ that we found was a $^3A_2'$, $(3e')^2$ state (hexagonal shape) with D_{3h} symmetry, and it had slightly higher energy than either of the $^1A_1$ isomers. Using the B3LYP

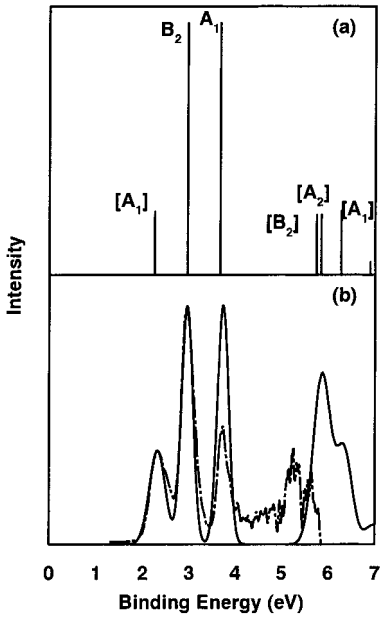

Figure 7. (a) Theoretical spectrum obtained using the calculated energies and pole strength values from MRSDCI calculations for $Al_3O_3^-$. The peaks have been shifted and scaled to make the first two peaks agree with experiment. (b) Comparison between the experimentally observed and theoretically derived photoelectron spectrum of $Al3O_3^-$. The dashed line represents the experimental spectrum and solid line represents the theoretical simulated spectrum.

calculated geometries of $Al_3O_2^-$ and $Al_3O_3^-$, configuration interaction calculations have been done to determine the low lying vertical excited states of Al_3O_2 and Al_3O_3. Those CI results along with the molecular orbital energy diagrams have been utilized to interpret the recently reported experimental photoelectron spectrum of $Al_3O_2^-$ and $Al3O_3^-$. In terms of peak positions and intensities, qualitative agreement is observed between the experimentally observed and the theoretically derived spectra of $Al_3O_2^-$ and $Al3O_3^-$. It has been found that for both $Al_3O_2^-$ and $Al_3O_3^-$ at least two isomers of each negative ion are necessary to explain the experimental spectra. On the basis of the present MRSDCI results, the photoelectron transitions involved in both the observed spectra have been assigned.

Acknowledgment. This work was supported by Grant CHE-9613944 from the National Science Foundation.

References and Notes

(1) Wilson, S. *Electron Correlation in Molecules*; Oxford University Press: New York, 1984.

(2) See, for example: Desjardins, S. J.; Bawagan, A. D. O.; Liu, Z. F.; Tan, K. H.; Yang, Y.; Davidson, E. R. *J. Chem. Phys* **1995**, *102*, 6385 and references therein.

(3) Bawagan, A. D. O.; Desjardins, S. J.; Dailey, R.; Davidson, E. R. *J. Chem. Phys*. **1997**, *107*, 4295.

(4) Moghaddam, M. S.; Desjardins, S. J.; Bawagan, A. D. O.; Tan, K. H.; Yang, Y.; Davidson, E. R. *J. Chem. Phys*. **1995**, *103*, 10537.

(5) Rolke, J.; Zheng, Y.; Brion, C. E.; Yang, Y. A.; Davidson, E. R. *Chem. Phys*. **1998**, *230*, 153.

(6) Bawagan, A. D. O.; Ghanty, T. K.; Davidson, E. R.; Tan, K. H. *Chem. Phys. Lett.* **1998**, *287*, 61.

(7) Ghanty, T. K.; Davidson, E. R. *Mol. Phys.* **1999**, *96*, 735.

(8) Ghanty, T. K.; Davidson, E. R. *J. Phys. Chem*. **1999**, *103*, 2867.

(9) Cederbaum, L. S.; Domcke, W.; Schirmer, J.; von Niessen, W. *Adv. Chem. Phys*. **1986**, *65*, 115.

(10) Baeck, K. K.; Bartlett, R. J. *J. Chem. Phys*. **1998**, *109*, 1334.

(11) Archibong, F. E.; St-Amant, A. *J. Phys. Chem.* **1999**, *103*, 1109.

(12) *Metal Clusters*; Moskovits, M., Ed.; Wiley: New York, 1986.

(13) *Physics and Chemistry of Small Clusters*; Jena, P., Rao, B. K., Khanna, S. N., Eds.; NATO Advanced Science Institutes Series 158; Plenum: New York, 1987.

(14) Cox, D. M.; Trevor, D. J.; Whitten, R. L.; Rohling, E. A.; Kaldor, A. J. *J. Chem. Phys.* **1986**, *84*, 4651.

(15) Kudo, H. *Nature* **1992**, *355* 432.

(16) Wang, S. L.; Ledingham, K. W. D.; Singhal, R. P. *J. Phys. Chem.* **1996**, *100*, 11282.

(17) Boldyrev, A. I.; Schleyer, P. v. R. *J. Am. Chem. Soc.* **1991**, *113*, 9045.

(18) Boldyrev, A. I.; Shamovsky, I. L.; Schleyer, P. v. R. *J. Am. Chem. Soc.* **1992**, *114*, 6469.

(19) Vyacheslav, V. G.; Niessen, W. v.; Boldyrev, A. I.; Schleyer, P. v. R. *Chem. Phys.* **1993**, *174*, 167.

(20) Boldyrev, A. I.; Simons, J.; Zakrzewski, V. G.; Niessen, W. v. *J. Phys. Chem.* **1994**, *98*, 1427.

(21) Schleyer, P. v. R.; Kapp, J. *Chem. Phys. Lett.* **1996,** *255*, 363.

(22) Wu, H.; Li, X.; Wang, X. B.; Ding, C. F.; Wang, L. S. *J. Chem. Phys.* **1998**, *109*, 449.

(23) Frisch, M. J.; Trucks, G. W.; Schlegel, H. B.; Scuseria, G. E.; Robb, M. A.; Cheeseman, J. R.; Zakrzewski, V. G.; Montgomery, Jr., J. A.; Stratmann, R. E.; Burant, J. C.; Dapprich, S.; Millam, J. M.; Daniels, A. D.; Kudin, K. N.; Strain, M. C.; Farkas, O.; Tomasi, J.; Barone, V.; Cossi, M.; Cammi, R.; Mennucci, B.; Pomelli, C.; Adamo, C.; Clifford, S.; Ochterski, J.; Peterson, G. A.; Ayala, P. Y.; Cui, Q.; Morokuma, K.; Malick, D. K.; Rabuck, A. D.; Raghavachari, K.; Foresman, J. B.; Cioslowski, J.; Ortiz, J. V.; Stefanov, B. B.; Liu, G.; Liashenko, A.; Piskorz, P.; Komaromi, I.; Gomperts, R.; Martin, R. L.; Fox, D. J.; Keith, T.; Al-Laham, M. A.; Peng, C. Y.; Nanayakkara, A.; Gonzalez, C.; Challacombe, M.; Gill, P. M. W.; Johnson, B.; Chen, W.; Wong, M. W.; Andres, J. L.; Gonzalez, C.; Head-Gordon, M.; Replogle, E. S.; Pople, J. A. *Gaussian 98*, revision A.6; Gaussian, Inc.: Pittsburgh, PA, 1998.

(24) Dunning, T. H., Jr. *J. Chem. Phys.* **1989**, *90*, 1007. Woon, D. E.; Dunning, T. H., Jr. *J. Chem. Phys.* **1993**, *98*, 1358. Kendall, R. A.; Dunning, T. H., Jr.; Harrison, R. J. *J. Chem. Phys.* **1992**, *96*, 6769. Basis sets were obtained from the Extensible Computational Chemistry Environment Basis Set Database, version 1.0, as developed and distributed by the Molecular Science Computing Facility, Environmental and Molecular Sciences Laboratory, which is part of the Pacific Northwest Laboratory, P.O. Box 999, Richland, WA 99352, and funded by the U.S. Department of Energy. The pacific Northwest Laboratory is a multiprogram laboratory operated by Battelle Memorial Institute for the U.S. Department of Energy under Contract DE-AC06-76RLO 1830. Contact David Feller, Karen Schuchardt, or Don Jones for further information.

(25) MELD is a set of electronic structure programs written by L. E. McMurchie, S. T. Elbert, S. R. Langhoff, and E. R. Davidson, with extensive modifications by D. Feller and D. C Rawlings.

(26) Feller, D.; Davidson, E. R. *J. Chem. Phys.* **1981**, *84*, 3977.

(27) Dupuis, M.; Marquez, A.; Davidson, E. R. *HONDO 95.6*; IBM Corporation, Neighborhood Road, Kingston, NY 12401, 1995.